Photonic Network Communications
https://doi.org/10.1007/s11107-019-00844-0

ORIGINAL PAPER

320 Gb/s all-optical XOR gate using semiconductor optical amplifier-Mach–Zehnder interferometer and delayed interferometer

Amer Kotb[1,2] · **Kyriakos E. Zoiros**[3] · **Chunlei Guo**[1,4]

Received: 17 August 2018 / Accepted: 23 February 2019

Abstract
All-optical exclusive OR (XOR) gate with semiconductor optical amplifier (SOA)-Mach–Zehnder interferometer (MZI) and delayed interferometer (DI) is demonstrated at 320 Gb/s through numerical simulation and analysis. The performance of the XOR gate is investigated and evaluated against the quality factor (QF). The obtained results indicate that placing the DI in series with the SOA-MZI renders acceptable QF of the XOR outcome at the target data rate, as opposed to the case without the DI, where the achievement of the same goal is not possible.

Keywords All-optical XOR gate · Semiconductor optical amplifier · Mach–Zehnder interferometer · Delayed interferometer

1 Introduction

All-optical (AO) gates are basic building units for the realization of photonic circuits, subsystems, and networks capable of operating only by means of light and hence relieved from the practical limitations and complications of opto-electronic conversions [1]. In particular, the exclusive OR (XOR) constitutes the flagship gate as it is involved in the accomplishment of many AO signal processing functionalities of fundamental and advanced level [2]. A technological approach that has widely been employed for implementing this important gate in the optical domain relies on incorporating semiconductor optical amplifiers (SOAs) as active nonlinear elements in interferometric arrangements [3] and in particular in the Mach–Zehnder interferometer (MZI) [4]. However, single-channel data rates scale well beyond 100 Gb/s to cope with the emergence of new bandwidth-hungry applications; this approach cannot keep pace with this trend due to SOAs' inherently slow gain recovery [5]. In order to deal with this issue in an affordable manner while still taking advantage of conventional SOA-based interferometric schemes' attractive features and established maturity, researchers have resorted to the passive solution of serially connecting a delayed interferometer (DI) at the output of the SOA-MZI-based XOR gate [6–8]. The DI exploits the information that is hidden in the phase of the switched signal [8], and through the subtraction of a temporally offset copy of this quantity from itself, it creates a window whose duration is determined solely by the DI shorter delay [9], thus masking the longer SOA recovery time and its concomitant negative impact on signal quality. Since the efficiency of this method has been tested up to 160 Gb/s [7], which soon or later is expected to be surpassed by the compelling needs of modern broadband applications, it would be a good idea to investigate whether the DI can still support the execution of Boolean XOR logic with an extended data rate margin being as twice as fast as that reported so far. To this aim, we take the opportunity to study, for the first time to our knowledge, the performance of an XOR gate realized at 320 Gb/s using a DI after a SOA-MZI. This is achieved through appropriate SOA [10] and DI [8] modeling, which allows to examine and assess the impact of critical operating parameters on

✉ Amer Kotb
amer@ciomp.ac.cn

✉ Chunlei Guo
guo@optics.rochester.edu

1 The Guo China-US Photonics Laboratory, Changchun Institute of Optics, Fine Mechanics, and Physics, Chinese Academy of Sciences, Changchun 130033, China

2 Department of Physics, Faculty of Science, University of Fayoum, Fayoum 63514, Egypt

3 Lightwave Communications Research Group, Department of Electrical and Computer Engineering, School of Engineering, Democritus University of Thrace, 67100 Xanthi, Greece

4 The Institute of Optics, University of Rochester, Rochester, NY 14627, USA

Published online: 14 March 2019

the XOR gate quality factor (QF). The obtained simulation results highlight the beneficial role of the DI, under the action of which the SOA-MZI XOR gate can be feasibly designed to exhibit an acceptable QF at 320 Gb/s, while this is not possible without the DI.

The rest of the paper is organized as follows: The XOR gate operating principle and modeling formulation are described in Sect. 2. The numerical results are presented and discussed in Sect. 3. Finally, Sect. 4 contains the concluding remarks.

2 All-optical XOR gate using SOA-MZI-DI

2.1 Operation principle

The schematic diagram and truth table of the XOR operation using a SOA-MZI in series with a DI are shown in Fig. 1.

Two data streams A and B of identical wavelength are injected into the SOA-MZI upper and lower arms, respectively. A continuous wave (CW) beam of a different wavelength in the vicinity of 1550 nm, which acts as the 'probe,' is injected into the SOA-MZI middle arm and is equally split by a 3 dB optical coupler (OC). Two wavelength selective couplers (WSCs) are used to combine the CW input first half with data A and the CW input second half with data B so that these signal pairs are launched into SOA1 and SOA2, respectively. Signals A and B induce a phase shift on their corresponding CW beam copy via the nonlinear effect of the cross-phase modulation (XPM). When both signals A and B are '0' or '1,' the SOA dynamics are not, or are identically, perturbed, respectively, so that the MZI remains balanced and the CW beam replicas do not experience a phase change. Consequently, signals A and B interfere destructively at the output OC and the outcome is null, i.e., '0.' But when A = '1' and B = '0,' and vice versa, the CW beam constituent, which travels along with the signal that is active, undergoes through XPM manifested in the corresponding SOA, a phase change. Thus, when the divided CW beams recombine at the output OC, they interfere constructively producing a '1.' An optical band-pass filter (OBPF) placed at the MZI exit rejects signals other than the switched one. In this manner, the physical result that is incurred by the binary combinations of data inputs A and B and imprinted on the CW probe coincides with the truth table of Boolean XOR logic, which is hence executed AO. During this operation, however, the SOAs in the MZI are driven by data whose binary content is alternated on a sub-Tb/s scale, thereby imposing a heavy strain on the gain dynamics of these devices. Due to this fact, the profile of the pulses that are switched at the XOR gate output becomes distorted. This problem can be alleviated by exploiting the information that is hidden in the phase of the switched signal [8]. This can be done by serially placing after the SOA-MZI XOR gate a DI, which has a relative delay, $\Delta\tau$, in one of its arms, and a phase bias, $\Delta\Phi$, in the other arm. The role of this module is to impart a phase difference between the direct and delayed versions of the incoming switched signal [9]. This action opens a phase window [8], which allows restoring the quality of the switched pulses. More specifically, for the spaces, which have a small phase content, the window is closed and the output of the DI is null so that these bits are extinguished. For the marks, on the other hand, the induced phase excursions are arranged through the proper selection of $\Delta\tau$ to lie within the created window. Then by suitably adjusting $\Delta\Phi$, the switched signal can be made to interfere with its lagging replica at the DI's output either destructively or constructively. In this manner, the higher marks can be clamped and the lower marks can be comparatively enhanced so that their peaks are ultimately equalized. Therefore, the DI can improve the performance of the XOR operation and make it better than if the SOA-MZI were not assisted by its beneficial action, as shown in Sect. 3.

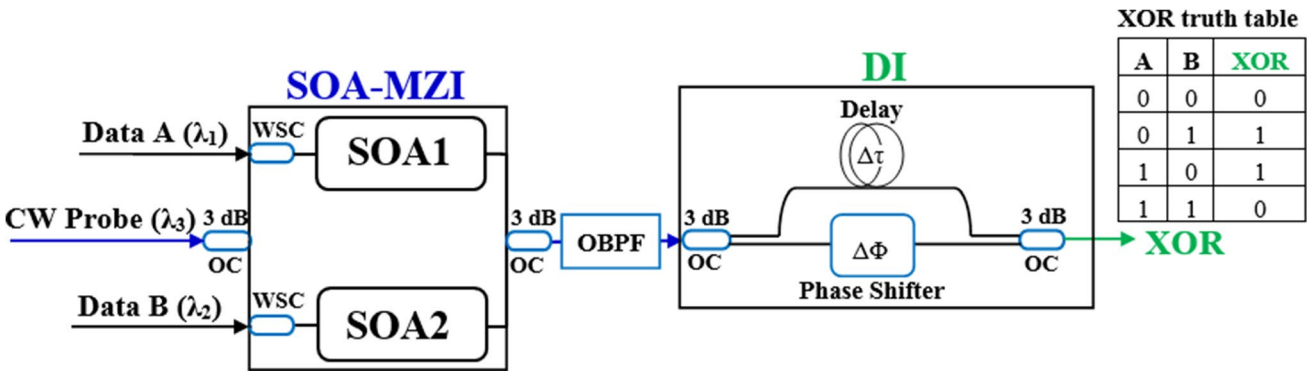

Fig. 1 Schematic diagram of XOR gate based on SOA-MZI in series with DI. *BPF* band-pass filter, *OC* 3 dB optical coupler, *WSC* wavelength selective coupler, *OBPF* optical band-pass filter

2.2 Simulation

The input signals A and B are assumed to exhibit a Gaussian-shaped power profile:

$$P_{A,B}(t) \equiv P_{\text{in}}(t) = \sum_{k=1}^{n} a_{k(A,B)} \frac{2\sqrt{\ln(2)}E_0}{\sqrt{\pi}\tau_{\text{FWHM}}} \exp\left[-\frac{4\ln(2)(t-kT)^2}{\tau_{\text{FWHM}}^2}\right] \tag{1}$$

where pulses have a full-width at half-maximum (FWHM) width, τ_{FWHM}, energy, E_0, and are positioned at k-th bit slots, $a_{k(A,B)}$, of binary content '1' or '0,' which are allocated within α pseudorandom binary sequence (PRBS) of length $n = 2^7 - 1$ [11]. The pulse format assumed in this simulation is the return-to-zero (RZ), which is widely employed in optical communications due to its attractive features of better tolerance to fiber nonlinearities and improved receiver sensitivity [12]. Pulses occupy only a fraction of the repetition interval, which helps avoid interference between adjacent allocated bit slots [13], and their generation while being as fast and short as in the conducted study is technologically feasible with lightwave sources developed for this purpose [14].

By considering the interband and intraband nonlinear effects, which include carrier depletion (CD), on the one hand, and carrier heating (CH) with spectral hole burning (SHB), on the other hand, the time-dependent gains of the SOAs inside the MZI are described by the following coupled differential equations [10, 15, 16]:

$$\frac{dh_{\text{CD}}(t)}{dt} = \frac{h_0 - h_{\text{CD}}(t)}{\tau_C} - (\exp[h_{\text{CD}}(t) + h_{\text{CH}}(t) + h_{\text{SHB}}(t)] - 1)\frac{P_{\text{in}}(t)}{E_{\text{sat}}} \tag{2}$$

$$\frac{dh_{\text{CH}}(t)}{dt} = -\frac{h_{\text{CH}}(t)}{\tau_{\text{CH}}} - \frac{\varepsilon_{\text{CH}}}{\tau_{\text{CH}}}(\exp[h_{\text{CD}}(t) + h_{\text{CH}}(t) + h_{\text{SHB}}(t)] - 1)P_{\text{in}}(t) \tag{3}$$

$$\frac{dh_{\text{SHB}}(t)}{dt} = -\frac{h_{\text{SHB}}(t)}{\tau_{\text{SHB}}} - \frac{\varepsilon_{\text{SHB}}}{\tau_{\text{SHB}}}(\exp[h_{\text{CD}}(t) + h_{\text{CH}}(t) + h_{\text{SHB}}(t)] - 1)P_{\text{in}}(t) - \frac{dh_{\text{CD}}(t)}{dt} - \frac{dh_{\text{CH}}(t)}{dt} \tag{4}$$

where function 'h' represents the SOAs' gains integrated over their length, which are induced during the dynamic processes of CD, CH, and SHB. Furthermore, $h_0 = \ln[G_0]$, where G_0 is the SOAs unsaturated power gain being directly proportional to their injection current, $E_{\text{sat}} = P_{\text{sat}}\,\tau_{\text{c}}$ is the SOAs saturation energy, where P_{sat} is the saturation power and τ_{c} is the carrier lifetime. $P_{\text{in}}(t)$ is the time-dependent power launched into the SOAs, which for each SOA is given by:

$$P_{\text{in,SOA}_1}(t) = P_A(t) + 0.5P_{\text{CW}} \tag{5}$$

$$P_{\text{in,SOA}_2}(t) = 0.5P_{\text{CW}} + P_B(t) \tag{6}$$

where P_{CW} is the CW input probe power. τ_{CH} and τ_{SHB} are the temperature relaxation rate and carrier–carrier scattering rate, respectively. ε_{CH} and ε_{SHB} are the nonlinear gain suppression factors due to CH and SHB, respectively.

The total gain, $G(t)$, of each SOA is given by [16]:

$$G(t) = \exp[(h_{\text{CD}}(t) + h_{\text{CH}}(t) + h_{\text{SHB}}(t))] \tag{7}$$

while the phase change, Φ(t), incurred on the signal propagating in each SOA is given by [16]:

$$\Phi(t) = -0.5\left(\alpha h_{\text{CD}}(t) + \alpha_{\text{CH}} h_{\text{CH}}(t) + \alpha_{\text{SHB}} h_{\text{SHB}}(t)\right) \tag{8}$$

where α is the traditional linewidth enhancement factor (α-factor) associated with CD, α_{CH} and α_{SHB} are the linewidth enhancement factors due to CH and SHB, respectively. α_{SHB} is zero because SHB produces a symmetrical spectral hole centered at the signal wavelength [10].

The XOR output power after the MZI is described by:

$$P_{\text{MZI}}(t) = 0.25P_{\text{CW}}(G_{\text{SOA1}}(t) + G_{\text{SOA2}}(t) - 2\sqrt{G_{\text{SOA1}}(t)G_{\text{SOA2}}(t)}\cos[\Phi_{\text{SOA1}}(t) - \Phi_{\text{SOA2}}(t)]) \tag{9}$$

where $G_{1,2}(t)$ and $\Phi_{1,2}(t)$ are the time-dependent gains and phase changes of the CW beam inside SOA1 and SOA2, respectively.

The XOR power at the output of the DI is described by [8]:

$$P_{\text{DI}}(t) = 0.25(P_{\text{MZI}}(t) + P_{\text{MZI}}(t - \Delta\tau) - 2\sqrt{P_{\text{MZI}}(t)P_{\text{MZI}}(t - \Delta\tau)}\cos[\Phi_{\text{XOR}}(t) - \Phi_{\text{XOR}}(t - \Delta\tau)] + \Delta\Phi) \tag{10}$$

where $\Delta\tau$ is the DI delay and $\Delta\Phi$ is the DI phase bias. $\Phi_{\text{XOR}}(t)$ is the SOA-MZI phase response explicitly expressed by [8]:

$$\Phi_{\text{XOR}}(t) = \Phi_{\text{SOA2}}(t) - \arctan\left[\frac{\sqrt{G_{\text{SOA1}}(t)/G_{\text{SOA2}}(t)}\,\sin\left[\Phi_{\text{SOA1}}(t) - \Phi_{\text{SOA2}}(t)\right]}{1 - \sqrt{G_{\text{SOA1}}(t)/G_{\text{SOA2}}(t)}\,\cos\left[\Phi_{\text{SOA1}}(t) - \Phi_{\text{SOA2}}(t)\right]}\right] \tag{11}$$

whose employment provides a more rigorous framework for studying AO XOR gates implemented with DI-assisted SOA-based interferometric schemes compared to previous numerical approaches followed for the same purpose [6, 7].

The effect of SOAs amplified spontaneous emission (ASE) is included by adding to the output power calculated from (11) or (12) the corresponding contribution [10]

$$P_{\text{ASE}} = N_{\text{sp}}\left(G_0 - 1\right) 2\pi\hbar\upsilon B_0 \tag{12}$$

where N_{sp} denotes the spontaneous emission factor, $\hbar$ is the normalized Planck's constant, B_0 is the optical bandwidth, and υ is the optical frequency.

To obtain acceptable XOR gate performance, the input signals' and SOAs' operating characteristics should be optimized. For this purpose, Eqs. (1)–(12) have been combined and incorporated in a computer program, which has been prepared and run in Mathematica® so as to obtain simulation results, using the involved parameters' values listed in Table 1. The values of the parameters considered as 'critical,' which include the SOAs' carrier lifetime, injection current, saturation power, and spontaneous emission factor, as well as the data signals' pulse energy and width and the DI delay, have been specified from the investigation of their impact on the defined performance metric, as detailed in the following section, while the values of the remaining parameters are typical ones [10, 11], [15, 16] and are assigned to them as 'default' throughout the simulation.

3 Results

The performance of the XOR gate using the SOA-MZI and DI is evaluated by means of the QF, which is defined as:

$$\mathrm{QF} = (P_1 - P_0)/(\sigma_1 + \sigma_0) \tag{13}$$

Table 1 Simulation parameters and values

Symbol	Parameter	Value	Unit
τ_c	Carrier lifetime	100	ps
α	Traditional linewidth enhancement factor	5	–
α_{CH}	Linewidth enhancement factor due to CH	1	–
α_{SHB}	Linewidth enhancement factor due to SHB	0	–
τ_{CH}	Temperature relaxation rate	0.3	ps
τ_{SHB}	Carrier–carrier scattering rate	0.1	ps
ε_{CH}	Nonlinear gain suppression factor due to CH	0.02	W^{-1}
ε_{SHB}	Nonlinear gain suppression factor due to SHB	0.02	W^{-1}
G_0	Unsaturated power gain	30	dB
P_{sat}	Saturation power	15	mW
I	Injection current	100	mA
λ_A	Wavelength of data A	1581	nm
λ_B	Wavelength of data B	1581	nm
λ_{CW}	Wavelength of CW probe	1540	nm
P_A	Power of data A	1	mW
P_B	Power of data B	1	mW
P_{CW}	Power of CW probe	2	mW
τ_{FWHM}	Pulse width	0.5	ps
E_0	Pulse energy	0.07	pJ
T	Bit period	3.125	ps
n	PRBS length	127	–
$\Delta\tau$	DI delay	0.2	ps
$\Delta\Phi$	DI phase bias	π	rad
N_{sp}	Spontaneous emission factor	2	–
B_0	Optical bandwidth	2	nm

where P_1, P_0 are the mean values of the logical '1's' and '0's' peak power at the SOA-MZI or DI output and σ_1, σ_0 are the corresponding standard deviations. For acceptable performance, the QF must exceed 6 (six) so as ensure a bit error rate less than 10^{-9} [15].

First, we specified the DI delay that maximizes the QF. As shown in Fig. 2, this happens for $\Delta\tau = 0.2$ ps.

Using this DI delay value, we investigated the impact of the SOAs' and data signals' critical parameters on the QF. This was done by progressively scanning each parameter while keeping the others constant with their respective values cited in Table 1. The set of simulation results obtained via this procedure is depicted in Figs. 3 and 4, which contain curves grouped for the case of SOA and data signals, respectively.

More specifically, Fig. 3a–d shows SOAs' carrier lifetime, injection current, saturation power, and spontaneous emission factor, while Fig. 4a and b shows pulses energy and width, respectively. From the observation of these figures, the following remarks can be made depending on whether the DI is used or not:

A. Without the DI

(i) The QF calculated for the combination of values assigned to the critical parameters according to Table 1 is less than the required minimum, i.e., QF = 4.5, and hence unacceptable.

(ii) It is not possible to raise the QF above six despite altering the SOAs carrier lifetime and spontaneous emission factor as well as data signals' pulse energy and width within their examined span. This means that these four parameters impose the tighter restrictions on the design of the AO logic scheme. In fact, changing them toward the direction that improves the QF corresponds to faster SOA gain recovery time, shorter data pulses duration, and less noisy SOA

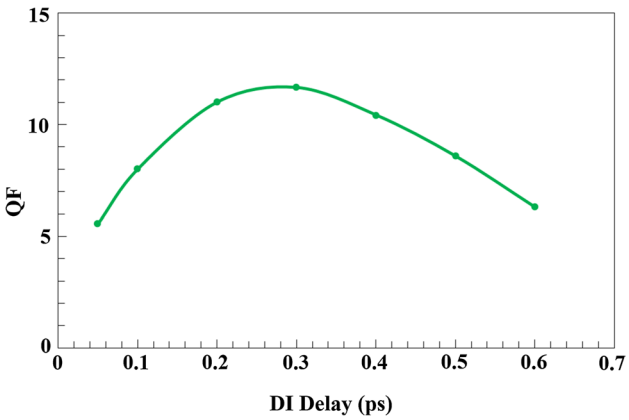

Fig. 2 QF versus delay of DI after SOA-MZI-based XOR gate at 320 Gb/s

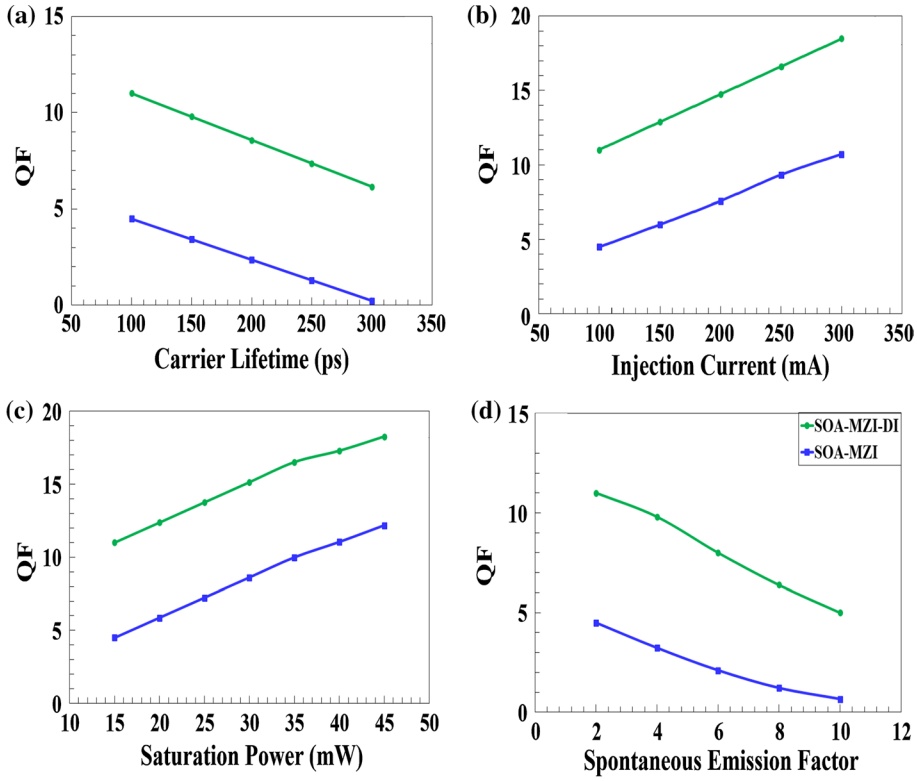

Fig. 3 QF versus (**a**) SOA carrier lifetime, **b** SOA injection current, **c** SOA saturation power, and **d** SOA spontaneous emission factor for SOA-MZI-DI- and SOA-MZI-based XOR operation at 320 Gb/s

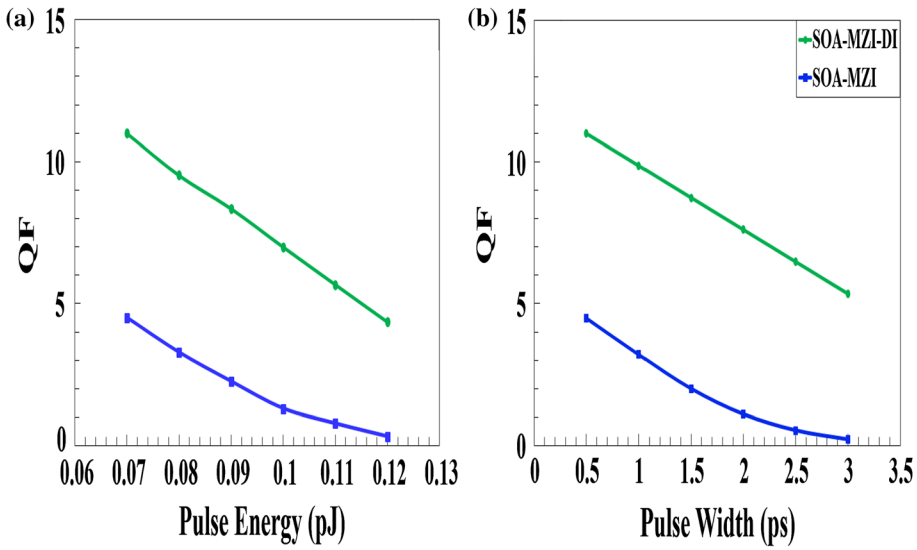

Fig. 4 QF versus data signals (**a**) pulse energy and **b** pulse width for SOA-MZI-DI- and SOA-MZI-based XOR operation at 320 Gb/s

behavior, which can be hard to achieve in practice, as well as to a narrower, hence undesirable, input power dynamic range.

(iii) It is possible to individually make the QF surpass its threshold by supplying SOAs with more carriers or raising the level at which they become saturated. These conditions are equivalent to increasing the SOA injection current or saturation power, respectively. This means that these parameters provide more freedom in the design of the AO XOR gate, however, at the inevitable expense of more energy-consuming current sources or erbium-doped fiber amplifiers.

B. With the DI

(iv) The QF calculated for the combination of values assigned to the critical parameters according to Table 1 is acceptable, i.e., QF = 11.

(v) In contrast to ii), it is now possible to render the QF acceptable. Additionally, this can be achieved for a wide span of the involved parameters, which can be

selected in a more relaxed and feasible manner. This allows SOAs to respond more slowly to ultrafast data pulses, whose energy can vary over a larger extent and width can be broader, while SOAs can tolerate more the inherently present noise.

(vi) Compared to (iii), the QF is now higher for the same parameter value. Unlike (iii), it is acceptable for lower parameters values, which means lower SOA bias current and saturation power and subsequently less electrical and power consumption.

The above points are directly reflected on the switched pulse profiles and eye diagrams obtained in each categorized case, I or II. Thus, Fig. 5 shows that the XOR logical outcome suffers from unacceptable [17] peak amplitude fluctuations as well as from the appearance at bit slots of small pulses where they should be extinguished. The eye diagram is deformed to analogous sub-envelopes of distorted shape, which degrade its quality. Nevertheless, Fig. 6 shows that these impairments are removed by the DI of optimized delay, since pulses occur according to the XOR truth table and exhibit equal amplitude, while the

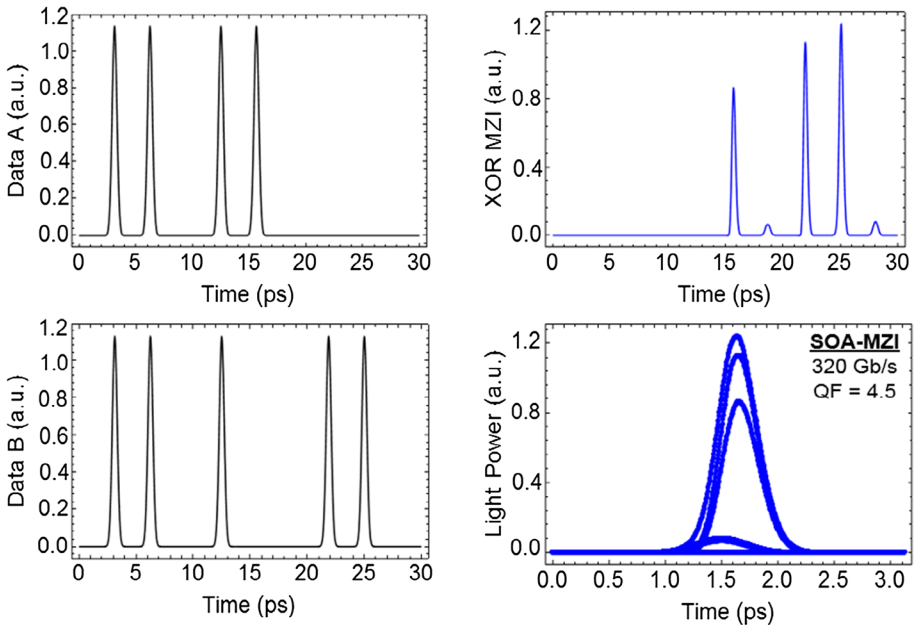

Fig. 5 Pulses' profile and eye diagram for XOR function at 320 Gb/s without DI after SOA-MZI

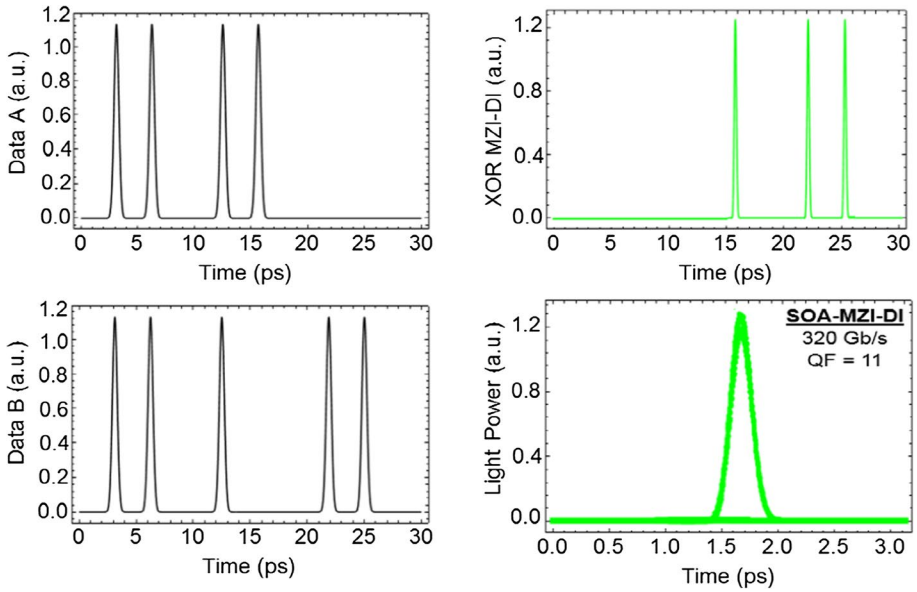

Fig. 6 Pulses' profile and eye diagram for XOR function at 320 Gb/s with DI after SOA-MZI

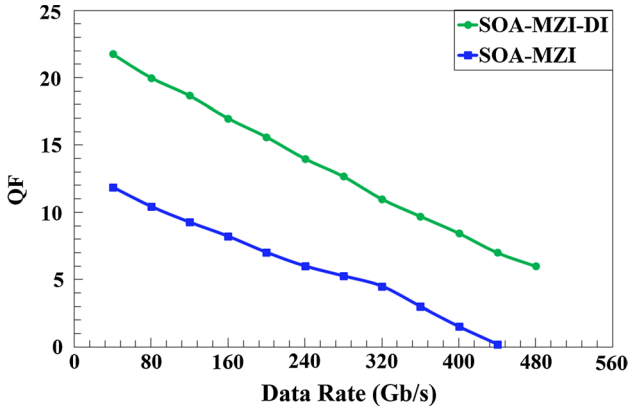

Fig. 7 QF versus SOA-MZI- and SOA-MZI-DI-based XOR gate data rate

corresponding eye diagram is restored, becoming clear and open with a single and uniform border.

The operation speed of the proposed XOR gate is determined by the DI delay. According to evidence acquired from studies on the performance of SOA devices, either stand-alone [18] or incorporated into interferometric arrangements [8], which utilize the assistance of this module to increase their ultrafast potential, the specific parameter should tend close to the data pulses full-width at half-maximum width and to about one-fourth of their repetition period, respectively. Thus, by applying these conditions and using the transitive property that holds through the DI delay, we can calculate that for a pulse duration of half picosecond used as default throughout the simulations the maximum data rate that can be supported by the proposed scheme is ~ 500 Gb/s. In fact, Fig. 7, which illustrates the QF dependence on the data rate, confirms this estimate, since the QF achieved at the rightmost extent of the horizontal axis is indeed acceptable.

The main factors for the experimental demonstration of the scheme are those that concern the practical availability of the data signals, SOAs, and DI according to the requirements specified through the theoretical study. Thus, the data signals launched into the SOA-MZI must have the appropriate intensity level, pulse width, and format at 320 Gb/s, which is possible with modern laser sources and erbium-doped fiber amplifiers for generating and boosting them, respectively [19]. Similarly, the SOAs must have physical characteristics and be driven under conditions which are affordable by off-the-shelf devices and their accompanying electronics [20]. Finally, the DI, which is mostly critical for achieving the considered AO logic operation at the target data rate, is also a commercially available module that can accurately provide the necessary sub-picosecond amount of delay [21]. Therefore, the realization of the proposed scheme is technologically feasible.

4 Conclusion

In conclusion, an all-optical logic XOR gate was theoretically demonstrated at a data rate of 320 Gb/s using a delayed interferometer (DI) after a semiconductor optical amplifier-Mach–Zehnder interferometer. The simulation results showed that owing to the DI the specific Boolean function can be executed in a technologically feasible manner with both logical correctness and high quality, whereas this is not possible without the DI.

References

1. Willner, A.E., Khaleghi, S., Chitgarha, M.R., Yilmaz, O.F.: All-optical signal processing. J. Lightwave Technol. **32**, 660–680 (2014)
2. Dimitriadou, E., Zoiros, K.E.: All-optical XOR gate using single quantum-dot SOA and optical filter. J. Lightwave Technol. **31**, 3813–3821 (2013)
3. Patel, N.S., Hall, K.L., Rauschenbach, K.A.: Interferometric all-optical switches for ultrafast signal processing. Appl. Opt. **37**, 2831–2842 (1998)
4. Zhang, M., Wang, L., Ye, P.: All-optical XOR logic gates: technologies and experiment demonstrations. IEEE Commun. Mag. **43**, S19–S24 (2005)
5. Mørk, J., Nielsen, M.L., Berg, T.W.: The dynamics of semiconductor optical amplifiers: Modeling and applications. Opt. Photon. News **14**, 42–48 (2003)
6. Sun, H., Wang, Q., Dong, H., Chen, Z., Dutta, N.K., Jaques, J., Piccirilli, A.B.: All-optical logic XOR gate at 80 Gb/s using SOA-MZI-DI. IEEE J. Quantum Electron. **42**, 747–751 (2006)
7. Randel, S., Melo, A.M., Petermann, K., Marembert, V., Schubert, C.: Novel scheme for ultrafast all-optical XOR operation. J. Lightwave Technol. **22**, 2808–2815 (2004)
8. Zoiros, K.E., Demertzis, C.: On the data rate extension of semiconductor optical amplifier-based ultrafast nonlinear interferometer in dual rail switching mode using a cascaded optical delay interferometer. Opt. Laser Technol. **43**, 1190–1197 (2011)
9. Gutiérrez-Castrejón, R., Dülk, M., Fischer, S., Guekos, G.: Novel scheme for optical time-division demultiplexing using a delayed interferometer. Opt. Commun. **192**, 245–254 (2001)
10. Kotb, A.: All-optical Logic Gates Using Semiconductor Optical Amplifier. Lambert Academic Publishing, Saarbrucken (2012)
11. Kotb, A., Zoiros, K.E., Guo, C.: 160 Gb/s photonic crystal semiconductor optical amplifiers-based all-optical logic NAND gate. Photon Netw. Commun. **36**, 246–255 (2018)
12. Breuer, D., Petermann, K.: Comparison of NRZ- and RZ-modulation format for 40-Gb/s TDM standard-fiber systems. IEEE Photon. Technol. Lett. **9**, 398–400 (1997)
13. Kawanishi, S.: Ultrahigh-speed optical time-division-multiplexed transmission technology based on optical signal processing. IEEE J. Quantum Electron. **34**, 2064–2079 (1998)
14. Zhu, G., Wang, Q., Chen, H., Dong, H., Dutta, N.K.: High-quality optical pulse train generation at 80 Gb/s using a modified regenerative-type mode-locked fiber laser. IEEE J. Quantum Electron. **40**, 721–725 (2004)
15. Dutta, N.K., Wang, Q.: Semiconductor Optical Amplifiers, 2nd edn. World Scientific Publishing Company, Singapore (2013)
16. Kotb, A., Zoiros, K.E., Guo, C.: All-optical XOR, NOR, and NAND logic functions with parallel semiconductor optical

amplifier-based Mach-Zehnder interferometer modules. Opt. Laser Technol. **108**, 426–433 (2018)
17. Vardakas, J.S., Zoiros, K.E.: Performance investigation of all-optical clock recovery circuit based on Fabry-Pérot filter and SOA-assisted Sagnac switch. Opt. Eng. **46**, 085005 (2007)
18. Zoiros, K.E., Siarkos, T., Koukourlis, C.S.: Theoretical analysis of pattern effect suppression in semiconductor optical amplifier utilizing optical delay interferometer. Opt. Commun. **281**, 3648–3657 (2008)
19. Mulvad, H.C.H., Galili, M., Oxenløwe, L.K., Hu, H., Clausen, A.T., Jensen, J.B., Peucheret, C., Jeppesen, P.: Demonstration of 5.1 Tb/s data capacity on a single-wavelength channel. Opt. Express **18**, 1438–1443 (2010)
20. Zimmerman, D.R., Spiekman, L.H.: Amplifiers for the masses: EDFA, EDWA, and SOA amplest for metro and access applications. J. Lightwave Technol. **22**, 63–70 (2004)
21. See for instance www.generalphotonics.com; www.ozoptics.com; www.santec.com

Amer Kotb has obtained the Ph.D. and M.Sc. in Electronics in 2012 and 2006, respectively. His Ph.D. thesis is carried out at University of Connecticut in the USA. He is currently an Associate Professor in Electronics in the Guo China-US Photonics Laboratory, Changchun Institute of Optics, Fine Mechanics, and Physics, Changchun 13003, China, and in the Department of Physics Faculty of Science, Fayoum University, Fayoum 63514, Egypt. Also, he worked as a visiting Professor in many countries. In 2019, Amer has obtained the Talented Young Scientist Program (TYSP) and the CAS President's International Fellowship Initiative (PIFI) supported by the Chinese Government. He has published as the first and corresponding author more than 35 international journal papers and one book in semiconductor optical amplifiers (SOAs)-based all-optical logic gates. His papers have been cited more than 330 with 12 h-index. He serves as a reviewer and an editorial member for a huge number of scientific journals. His current research activities are all-optical logic gates, SOAs, and computaional photonics at high data rates.

Kyriakos E. Zoiros received the Diploma in Electrical and Computer Engineering in 1996 and the Ph.D. in optical communications in 2000. He is currently an Associate Professor in the Department of Electrical and Computer Engineering, Democritus University of Thrace, Xanthi, Greece. In spring 2009, he was on leave at the Optical Communications Research Group, University of Limerick, Ireland. In fall 2013, he was on leave at the Laboratoire en Sciences et Techniques de l'Information, de la Communication et de la Connaissance (LabSTICC), École Nationale d'Ingénieurs de Brest, France. He has authored or co-authored more than 100 international journal and conference papers and 5 book chapters. His current research interests include all-optical signal processing, semiconductor optical amplifiers, microwave photonics, microring resonators and computational photonics.

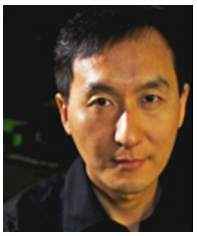

Chunlei Guo is the director of the Guo China-US Photonics Laboratory in Changchun Institute of Optics, Fine Mechanics, and Physics, Changchun 13003, China. Prof. Guo's research interests focus on laser–matter interactions at high intensities, nanophotonics, femtosecond laser surface nano- and microstructure, and surface plasmonics. He and his coworkers invented the so-called black and colored metals, which have a broad range of technological applications and have been covered extensively by the media. He is an elected Fellow for American Physical Society, Optical Society of America, and International Academy of Photonics and Laser Engineering. He serves as an editor and on editorial boards for a number of scientific journals and is the past Chair of Short-Wavelength and High-Field Physics Group in the Optical Society of America.